LUND UNIVERSITY

Multi-User Processing for Ray-Based Channels

Miller, Chelsea; Dmochowski, Pawel A; Smith, Peter J; Tataria, Harsh; Matthaiou, Michail

Multi-User Processing for Ray-Based Channels

Chelsea L. Miller*, Pawel A. Dmochowski*, Peter J. Smith†, Harsh Tataria‡, and Michail Matthaiou‡

* School of Engineering and Computer Science, Victoria University of Wellington, Wellington, New Zealand
†School of Mathematics and Statistics, Victoria University of Wellington, Wellington, New Zealand
‡Institute of Electronics, Communications and Information Technology (ECIT), Queen's University Belfast, Belfast, U.K.
email: {chelsea.miller,pawel.dmochowski}@ecs.vuw.ac.nz, peter.smith@vuw.ac.nz, {h.tataria,m.matthaiou}@qub.ac.uk

Abstract—The performance of linear multi-user multiple-input multiple-output (MU-MIMO) systems has been extensively studied for *classical statistical* channel models. In contrast, there is little analysis for *ray-based* models, which are physically motivated, feature prominently in standards and have been experimentally validated. Thus, we present a novel analysis framework for zero forcing (ZF) and maximal ratio combining (MRC) applicable to such models. Specifically, using a central result for averaging in the angular domain, we derive accurate expressions for ZF signal-to-noise ratio and MRC signal, interference and noise powers. The remarkably simple expressions offer the following insights into the effects of the propagation environment. While ZF is robust to parameters such as cluster and subray angle spreads, MRC interference is highly sensitive to them. We show that the performance scales linearly with the number of antennas, and that it degrades with narrow angle spreads and as the propagation moves toward the antenna end-fire. Finally, by evaluating the variance of the MRC interference, we observe that an approximation to the MRC SINR widely used for classical statistical models, is inaccurate in ray-based channels.

I. INTRODUCTION

Theoretical performance analysis of linear processing schemes for multi-user multiple-input multiple-output (MU-MIMO) is extremely well advanced for classical statistical channel models. Early work on Rayleigh fading channels has been extended to a wide range of more complex and realistic channels. For example, results are now emerging on complex, heterogeneous, correlated Rician channels for both uplink (UL) and downlink (DL) systems employing maximal ratio combining (MRC) [1], zero-forcing (ZF) [2] and minimum square error (MMSE) combining [3], [4]. In contrast, the literature on performance analysis for ray-based channels is very sparse. In this paper, we use the phrase *ray-based* to denote a wide class of channel models where a user's channel is broken down into rays and the angles of the rays are specified by some statistical distribution. This covers many of the models described as spatial, directional or geometric.

Ray-based models have several advantages over the classical statistical channel models: they are more physically based; have a direct link to the antenna layout and the propagation environment; and apply over a wide range of frequencies. For example, recent ray-based measurements are used to characterize the channel at 2.53 GHz [5] and at 28 GHz and 73 GHz [6]. For these reasons, ray-based channels form the basis of many standardized models [7].

However, the mathematical difficulties attached to such models have obstructed the progress in the analysis of these types of channels. Many papers therefore necessarily focus on simulation [8], [9]. Some analysis of ray-based models in regard to favorable propagation and channel hardening has appeared in [10]–[12]. Furthermore, [13] analyzes the achievable rate with maximal ratio transmission (MRT) in downlink transmissions. The bulk of the work to date makes restrictive assumptions regarding the ray angles and their angular distributions. For example, it is often assumed that the ray angles [10] or the sine of the ray angles [13], [14] are uniform over $[0, 2\pi]$. More recently, work has appeared on DL conjugate beamforming and regularized ZF [15] with pilot contamination but again the angles are restricted to be uniform.

It is clear that the performance analysis methodology for such channels is in its infancy and is extremely challenging. For this reason, the methodology developed here focuses on the initial case of a single cell and perfect channel state information (CSI). Although exact analysis of linear processing in MU-MIMO systems is almost certainly intractable, we note that moment-based approaches are promising for moderate to large systems and for massive MIMO. This observation is based on the fact that expectations of cross products of channels are the building blocks of the analysis of favorable propagation, channel hardening, MRT and MRC. This is the area where most analytical work has made progress. Further, we note that moment based approaches were used successfully in [1]–[4] for complex statistical channel models.

Hence, in this paper we develop a novel methodology to analyze MRC and ZF in UL systems for an extremely wide range of ray distributions. This includes all commonly used ray models, such as those containing clusters of rays and angles with wrapped Gaussian and Laplacian distributions. Hence, this work is considerably more general than previous work in the area. In particular we make the following contributions:

- We derive an accurate approximation to the mean signal-to-noise ratio (SNR) of ZF;
- We derive exact results for the mean signal power, interference power and noise power of MRC;
- We demonstrate that the high variance of the interference in MRC makes traditional signal-to-interference-and-noise ratio (SINR) approximations inaccurate;
- We provide remarkably simple, closed form results which deliver many insights into the link between performance

and the system parameters and ray distributions;

- Specific conclusions from the analysis verified by simulation include: the robustness of ZF to angular parameters; the sensitivity of MRC to angular parameters; the fact that performance scales linearly with antenna numbers and the performance degradation that occurs with limited angle spread or a shift in the ray angles away from broadside.

II. SYSTEM MODEL

We examine a single-cell MU-MIMO system where a centrally located base station (BS) with an M-antenna uniform linear array (ULA) serves L single-antenna users within a single resource block. We consider UL transmission assuming perfect channel knowledge at the BS.

A. Channel Model

The $M \times 1$ channel vector between the BS and the lth user is modeled by the generic clustered ray-based model:

$$\mathbf{h}_l = \sum_{c=1}^{C} \sum_{s=1}^{S} \gamma_{c,s}^{(l)} \mathbf{a}(\phi_{c,s}^{(l)}), \tag{1}$$

where C is the number of clusters and S is the number of subpaths per cluster. The vector $\mathbf{a}(\phi_{c,s}^{(l)}) = [1, e^{j2\pi\delta \sin \phi_{c,s}^{(l)}} \dots e^{j2\pi(M-1)\delta \sin \phi_{c,s}^{(l)}}]^T$ represents the $M \times 1$ steering vector pertaining to subray s in cluster c sent from user l, and δ is the antenna spacing in wavelengths. The angle of arrival (AoA) of each ray is modeled as $\phi_{c,s}^{(l)} = \phi_c^{(l)} + \Delta_{c,s}^{(l)}$ with $\phi_c^{(l)}$ being the central angle of the rays of cluster c, and $\Delta_{c,s}^{(l)}$ being the deviation of ray s from that central angle. The ray coefficients, $\gamma_{c,s}^{(l)}$, are modeled as $\gamma_{c,s}^{(l)} = \beta_{c,s}^{(l)1/2} e^{j\theta_{c,s}^{(l)}}$ where $\beta_{c,s}^{(l)}$ is the ray power and $\theta_{c,s}^{(l)} \sim \mathcal{U}[0, 2\pi]$ are uniform phases. Hence, the total link gain for user l is $\beta^{(l)} = \sum_{c=1}^{C} \sum_{s=1}^{S} \beta_{c,s}^{(l)}$. The classical path-loss and shadowing model is used for the link gains so that

$$\beta^{(l)} = AX_l \left(\frac{d_l}{d_0} \right)^{-\Gamma}, \tag{2}$$

where d_l is the distance between user l and the BS, A is the received power at the reference distance d_0 in the absence of shadowing, Γ is the pathloss exponent, and X_l models the effects of shadow fading, taken from a lognormal distribution with zero mean and variance σ_{sf}^2.

B. SINR and Spectral Efficiency

The received signal at the BS can be written as

$$\mathbf{y} = \rho^{\frac{1}{2}} \mathbf{H} \mathbf{s} + \mathbf{n}, \tag{3}$$

where ρ is the uplink transmit power (assumed equal for all users), $\mathbf{H} = [\mathbf{h}_1, \mathbf{h}_2, ..., \mathbf{h}_L]$ is the $M \times L$ composite channel matrix and $\mathbf{s} = [s_1, s_2, ..., s_L]^T$, is the vector of user symbols, with $\mathbb{E}[s_i] = 0$ and $\mathbb{E}[|s_i|^2] = 1$. The additive white Gaussian noise at the receiver is $\mathbf{n} \sim \mathcal{CN}(\mathbf{0}, \sigma_n^2 \mathbf{I_M})$. This received signal

is processed using a ZF or MRC linear receiver at the BS, producing for user l the signal

$$y_l = \rho^{\frac{1}{2}} \mathbf{w}_l^H \mathbf{h}_l s_l + \sum_{l' \neq l}^{L} \rho^{\frac{1}{2}} \mathbf{w}_l^H \mathbf{h}_{l'} s_{l'} + \mathbf{w}_l^H \mathbf{n}. \tag{4}$$

The weight vector for user l, $\mathbf{w}_l$, is the lth column of the matrix:

$$\mathbf{W}^{\text{MRC}} \triangleq \mathbf{H}, \tag{5}$$

$$\mathbf{W}^{\text{ZF}} \triangleq \mathbf{H}(\mathbf{H}^H \mathbf{H})^{-1}, \tag{6}$$

for MRC or ZF, respectively. The resulting SINR is:

$$\text{SINR}_l = \frac{\rho |\mathbf{w}_l^H \mathbf{h}_l|^2}{\rho \sum_{l' \neq l}^{L} |\mathbf{w}_l^H \mathbf{h}_{l'}|^2 + \sigma_n^2 \|\mathbf{w}_l\|^2}, \tag{7}$$

leading to the spectral efficiency: $\text{SE}_l = \log_2(1 + \text{SINR}_l)$.

III. AVERAGE SINR AND SPECTRAL EFFICIENCY

We examine the ergodic cell-wide SE of an arbitrary user, l, by first analyzing the expectation over the ray angles, $\phi_{c,s}^{(l)}$, and phases, $\theta_{c,s}^{(l)}$. Hence, we average throughout the paper over all the variables in the channel except for the ray powers, $\beta_{c,s}^{(l)}$. This approach is used for two reasons. First, it leads to expressions where the effects of the ray powers can be seen. Secondly, there are a wide variety of models for the $\beta_{c,s}^{(l)}$ terms so further averaging is best done on a case-by-case basis or by simulation. The expected SE is simplified with the following common approximation

$$\mathbb{E}_{\theta,\phi}[\text{SE}_l] \approx \log_2(1 + \mathbb{E}_{\theta,\phi}[\text{SINR}_l]), \tag{8}$$

where $\mathbb{E}_{\theta,\phi}[\cdot]$ refers to expectation over the ray angles and the phases of the ray coefficients. Hence, we derive expressions for $\mathbb{E}_{\theta,\phi}[\text{SINR}_l]$ for MRC and ZF processing.

A. MRC Processing

By substituting the MRC weighting vector in (5) into (7), we see that the SINR for user l is

$$\text{SINR}_l^{\text{MRC}} = \frac{\rho |\mathbf{h}_l^H \mathbf{h}_l|^2}{\rho \sum_{l' \neq l}^{L} |\mathbf{h}_l^H \mathbf{h}_{l'}|^2 + \sigma_n^2 \|\mathbf{h}_l\|^2}. \tag{9}$$

Averaging the SINR over the AoAs and ray phases is facilitated by the following approximation [1], [2], [16]

$$\mathbb{E}_{\theta,\phi}[\text{SINR}_l^{\text{MRC}}] \approx \frac{\rho \mathbb{E}_{\theta,\phi}[|\mathbf{h}_l^H \mathbf{h}_l|^2]}{\rho \sum_{l' \neq l}^{L} \mathbb{E}_{\theta,\phi}[|\mathbf{h}_l^H \mathbf{h}_{l'}|^2] + \sigma_n^2 \mathbb{E}_{\theta,\phi}[\|\mathbf{h}_l\|^2]}. \tag{10}$$

The approximation in (10) is of the form $\mathbb{E}[X/Y] \approx \mathbb{E}[X]/\mathbb{E}[Y]$, which has been shown to be accurate for moderate to large M, and relies on Y having a small variance relative to its mean [16], a condition satisfied for classical channel models. In Section V, we thus examine the variability in the MRC interference in ray-based channels, demonstrating that in some cases it exhibits large fluctuations, making the approximation less accurate than in classical channel models.

1) Signal: To derive the expected signal power we require

$$\mathbb{E}_{\theta,\phi}[|\mathbf{h}_l^H \mathbf{h}_l|^2] = \mathbb{E}_{\theta,\phi}\left[\left|\sum_{c,s}^{C,S}\sum_{\hat{c},\hat{s}}^{C,S}\gamma_{c,s}^{(l)*}\gamma_{\hat{c},\hat{s}}^{(l)}\mathbf{a}^H(\phi_{c,s}^{(l)})\mathbf{a}(\phi_{\hat{c},\hat{s}}^{(l)})\right|^2\right]$$

$$= \mathbb{E}_{\theta,\phi}\left[\sum_{c,s}^{C,S}\sum_{\hat{c},\hat{s}}^{C,S}\sum_{c',s'}^{C,S}\sum_{\hat{c}',\hat{s}'}^{C,S}\gamma_{c,s}^{(l)*}\gamma_{\hat{c},\hat{s}}^{(l)}\gamma_{c',s'}^{(l)*}\gamma_{\hat{c}',\hat{s}'}^{(l)}\right.$$

$$\left.\times \mathbf{a}^H(\phi_{c,s}^{(l)})\mathbf{a}(\phi_{\hat{c},\hat{s}}^{(l)})\mathbf{a}^H(\phi_{c',s'}^{(l)})\mathbf{a}(\phi_{\hat{c}',\hat{s}'}^{(l)})\right]$$

$$= M^2\sum_{c,s}^{C,S}\mathbb{E}_{\theta,\phi}\left[|\gamma_{c,s}^{(l)}|^4\right]+\sum_{c,s}^{C,S}\sum_{\hat{c},\hat{s}\neq c,s}^{C,S}\beta_{c,s}^{(l)}\beta_{\hat{c},\hat{s}}^{(l)}\mathbb{E}_{\theta,\phi}\left[|\mathbf{a}^H(\phi_{c,s}^{(l)})\mathbf{a}(\phi_{\hat{c},\hat{s}}^{(l)})|^2\right]$$

$$+ M^2\sum_{c,s}^{C,S}\sum_{c',s'\neq c,s}^{C,S}\beta_{c,s}^{(l)}\beta_{c',s'}^{(l)} \triangleq T_1 + T_2 + T_3, \quad (11)$$

where $\sum_{c,s}^{C,S} = \sum_{c=1}^{C}\sum_{s=1}^{S}$. The simplifications in (11) follow from properties of the ray power statistics, namely: $\mathbb{E}_{\theta,\phi}[\gamma_{c_1,s_1}^{(l_1)*}\gamma_{c_2,s_2}^{(l_2)}] = 0$ for all cases except $c_1 = c_2, s_1 = s_2, l_1 = l_2$ (i.e. the same user-cluster-subray combination). This logic recurs throughout the remaining derivations. The middle term in (11), T_2, requires two expectations according to whether $c = \hat{c}$ or $c \neq \hat{c}$. Breaking T_2 into these two cases gives $T_2 = K_c\epsilon_c^{(l)} + K_s\epsilon_s^{(l)}$, where $\epsilon_c^{(l)} = \beta^{(l)2} - \sum_{c=1}^{C}\beta_c^{(l)2}$, $\epsilon_s^{(l)} = \sum_{c=1}^{C}\beta_c^{(l)2} - \sum_{c,s}^{C,S}\beta_{c,s}^{(l)2}$ and $\beta_c^{(l)}$ is the cluster power, $\beta_c^{(l)} = \sum_{s=1}^{S}\beta_{c,s}^{(l)}$. The constants K_c and K_s relate to the ray angle distribution and are defined below. First, K_c is given by

$$K_c\triangleq\mathbb{E}_{\phi}\left[|\mathbf{a}^H(\phi_{c,s}^{(l)})\mathbf{a}(\phi_{\hat{c},\hat{s}}^{(l)})|^2\right]=\sum_{m=0}^{M-1}\sum_{m'=0}^{M-1}|\mathbb{E}_{\phi}[e^{j2\pi\delta(m'-m)\sin\phi}]|^2, \quad (12)$$

which follows because distinct rays are i.i.d. and $(c,s) \neq (\hat{c},\hat{s})$. Secondly, K_s is given by

$$K_s \triangleq \mathbb{E}_{\phi}\left[|\mathbf{a}^H(\phi_{c,s}^{(l)})\mathbf{a}(\phi_{c,\hat{s}}^{(l)})|^2\right]$$

$$= \sum_{m=0}^{M-1}\sum_{m'=0}^{M-1}|\mathbb{E}_{\phi}[e^{j2\pi\delta(m'-m)(\sin\phi_{c,\hat{s}}^{(l)}-\sin\phi_{c,s}^{(l)})}]|^2. \quad (13)$$

Further details of the numeric computation of K_c and K_s are given in Sec. IV. Finally, noting that $T_1 + T_2 = M^2\beta^{(l)2}$,

$$\mathbb{E}_{\phi}[|\mathbf{h}_l^H \mathbf{h}_l|^2] = M^2\beta^{(l)2} + K_c\epsilon_c^{(l)} + K_s\epsilon_s^{(l)}. \quad (14)$$

2) Interference: The expected interference power requires

$$\mathbb{E}_{\theta,\phi}\left[|\mathbf{h}_l^H \mathbf{h}_{l'}|^2\right] = \mathbb{E}_{\theta,\phi}\left[\sum_{c,s}^{C,S}\sum_{\hat{c},\hat{s}}^{C,S}\sum_{c',s'}^{C,S}\sum_{\hat{c}',\hat{s}'}^{C,S}\gamma_{c,s}^{(l)*}\gamma_{\hat{c},\hat{s}}^{(l)}\gamma_{c',s'}^{(l')*}\gamma_{\hat{c}',\hat{s}'}^{(l')}\right.$$

$$\left.\times \mathbf{a}^H(\phi_{c,s}^{(l)})\mathbf{a}(\phi_{\hat{c}',\hat{s}'}^{(l')})\mathbf{a}^H(\phi_{c',s'}^{(l')})\mathbf{a}(\phi_{\hat{c},\hat{s}}^{(l)})\right]$$

$$= \sum_{c,s}^{C,S}\sum_{c',s'}^{C,S}\beta_{c,s}^{(l)}\beta_{c',s'}^{(l')}\mathbb{E}\left[|\mathbf{a}^H(\phi_{c,s}^{(l)})\mathbf{a}(\phi_{c',s'}^{(l')})|^2\right]$$

$$= K_c\sum_{c,s}^{C,S}\sum_{c',s'}^{C,S}\beta_{c,s}^{(l)}\beta_{c',s'}^{(l')} = K_c\beta^{(l)}\beta^{(l')}. \quad (15)$$

3) Noise: Finally, to compute the noise power, we require:

$$\mathbb{E}_{\theta,\phi}\left[\|\mathbf{h}_l\|^2\right] = \mathbb{E}_{\theta,\phi}\left[\sum_{c,s}^{C,S}\sum_{\hat{c},\hat{s}}^{C,S}\gamma_{c,s}^{(l)*}\gamma_{\hat{c},\hat{s}}^{(l)}\mathbf{a}^H(\phi_{c,s}^{(l)})\mathbf{a}(\phi_{\hat{c},\hat{s}}^{(l)})\right]$$

$$= \sum_{c,s}^{C,S}\beta_{c,s}^{(l)}\mathbb{E}_{\phi}\left[\mathbf{a}^H(\phi_{c,s}^{(l)})\mathbf{a}(\phi_{c,s}^{(l)})\right] = \sum_{c,s}^{C,S}\beta_{c,s}^{(l)}M = M\beta^{(l)}. \quad (16)$$

Substituting (14), (15), and (16) into (9), gives the final closed-form approximation for the MRC SINR of user l, (17), given at the top of the following page. Note that (17) gives the mean SINR approximation solely in terms of the powers and the two expectations in (12) and (13), derived in Sec. IV.

B. ZF Processing

It is well known that the ZF SINR can be written as

$$\text{SINR}_l^{\text{ZF}} = \frac{\rho}{((\mathbf{H}^H\mathbf{H})^{-1})_{l,l}}. \quad (18)$$

Via the approximation motivated and verified in [2], we write

$$\mathbb{E}_{\theta,\phi}[\text{SINR}_l^{\text{ZF}}] \approx \frac{\rho}{\mathbb{E}_{\theta,\phi}[((\mathbf{H}^H\mathbf{H})^{-1})_{l,l}]}. \quad (19)$$

Since the matrix inverse in (19) is intractable for ray-based models, we adopt the Neumann series approach in [2]. We write the matrix inverse in the denominator of (18) as:

$$(\mathbf{H}^H\mathbf{H})^{-1} = (\mathbb{E}_{\theta,\phi}[\mathbf{H}^H\mathbf{H}] + \mathbf{H}^H\mathbf{H} - \mathbb{E}_{\theta,\phi}[\mathbf{H}^H\mathbf{H}])^{-1}$$

$$= (\mathbf{X} + \mathbf{X}')^{-1} = (\mathbf{I}_L + \mathbf{X}^{-1}\mathbf{X}')^{-1}\mathbf{X}^{-1} \quad (20)$$

where $\mathbf{X} = \mathbb{E}_{\theta,\phi}[\mathbf{H}^H\mathbf{H}]$ and $\mathbf{X}' = \mathbf{H}^H\mathbf{H} - \mathbb{E}_{\theta,\phi}[\mathbf{H}^H\mathbf{H}]$. As seen in [2] and [17], (20) can be approximated using a second-order Neumann approximation.

$$\mathbb{E}_{\theta,\phi}[(\mathbf{I}_L + \mathbf{X}^{-1}\mathbf{X}')^{-1}\mathbf{X}^{-1}] \approx$$

$$\mathbb{E}_{\theta,\phi}[(\mathbf{I}_L - \mathbf{X}^{-1}\mathbf{X}' + \mathbf{X}^{-1}\mathbf{X}'\mathbf{X}^{-1}\mathbf{X}')\mathbf{X}^{-1}]$$

$$= \mathbf{X}^{-1} - \mathbf{0} + \mathbf{X}^{-1}\mathbb{E}_{\theta,\phi}[\mathbf{X}'\mathbf{X}^{-1}\mathbf{X}']\mathbf{X}^{-1}, \quad (21)$$

using $\mathbb{E}_{\theta,\phi}[\mathbf{X}'] = \mathbb{E}_{\theta,\phi}[\mathbf{H}^H\mathbf{H} - E_{\theta,\phi}[\mathbf{H}^H\mathbf{H}]] = 0$, and the fact that $\mathbf{X}$ is deterministic. Expanding the expectation in (21) and simplifying, we obtain:

$$\mathbb{E}_{\theta,\phi}[(\mathbf{H}^H\mathbf{H})^{-1}]_{l,l} \approx [\mathbf{X}^{-1}\mathbb{E}_{\theta,\phi}[\mathbf{H}^H\mathbf{H}\mathbf{X}^{-1}\mathbf{H}^H\mathbf{H}]\mathbf{X}^{-1}]_{l,l}$$

$$= \mathbf{X}_{l,l}^{-1}\mathbb{E}_{\theta,\phi}[\mathbf{H}^H\mathbf{H}\mathbf{X}^{-1}\mathbf{H}^H\mathbf{H}]_{l,l}\mathbf{X}_{l,l}^{-1}, \quad (22)$$

which follows since $\mathbf{X} = \mathbb{E}_{\theta,\phi}[\mathbf{H}^H\mathbf{H}]$ is diagonal. Through a similar process to that in (14), (15), and (16), we have:

$$\mathbb{E}_{\theta,\phi}[(\mathbf{H}^H\mathbf{H}\mathbf{X}^{-1}\mathbf{H}^H\mathbf{H})_{l,l}] =$$

$$\mathbb{E}_{\theta,\phi}\left[\sum_{l'=1}^{L}(\mathbf{h}_l^H\mathbf{h}_{l'})(\mathbf{X}^{-1})_{l',l'}(\mathbf{h}_{l'}^H\mathbf{h}_l)\right]$$

$$= \sum_{l'=1}^{L}\frac{1}{M\beta^{(l')}}E_{\theta,\phi}\left[\sum_{c,s}^{C,S}\sum_{\hat{c},\hat{s}}^{C,S}\sum_{c',s'}^{C,S}\sum_{\hat{c}',\hat{s}'}^{C,S}\gamma_{c,s}^{(l)*}\gamma_{\hat{c},\hat{s}}^{(l')}\gamma_{c',s'}^{(l')*}\gamma_{\hat{c}',\hat{s}'}^{(l)}\right.$$

$$\left.\times \mathbf{a}^H(\phi_{c,s}^{(l)})\mathbf{a}(\phi_{\hat{c},\hat{s}}^{(l')})\mathbf{a}^H(\phi_{c',s'}^{(l')})\mathbf{a}(\phi_{\hat{c}',\hat{s}'}^{(l)})\right]$$

$$= K_c\left(L\frac{\beta^{(l)}}{M} - \frac{1}{M\beta^{(l)}}\sum_{c,s}^{C,S}\beta_{c,s}^{(l)2}\right) + M\beta^{(l)}, \quad (23)$$

$$\mathbb{E}_{\theta,\phi}[\text{SINR}_l^{\text{MRC}}] \approx \frac{\rho \left\{ M^2 \beta^{(l)2} + K_c \epsilon_c^{(l)} + K_s \epsilon_s^{(l)} \right\}}{\rho K_c \sum_{l' \neq l}^{L} \beta^{(l)} \beta^{(l')} + \sigma_n^2 M \beta^{(l)}} \tag{17}$$

where we substituted $(\mathbf{X}^{-1})_{l,l} = ((\mathbb{E}_{\theta,\phi}[\mathbf{H}^H \mathbf{H}])^{-1})_{l,l} = \frac{1}{M\beta^{(l)}}$ using (16). Substituting (23) and (16) into (22) gives

$$\mathbb{E}_{\theta,\phi}[(\mathbf{H}^H \mathbf{H})^{-1}]_{l,l}$$
$$\approx \left(\frac{1}{M\beta^{(l)}} \right)^2 \left[K_c \left(L \frac{\beta^{(l)}}{M} - \frac{1}{M\beta^{(l)}} \sum_{c,s}^{C,S} \beta_{c,s}^{(l)2} \right) + M\beta^{(l)} \right]. \tag{24}$$

Hence, the closed-form approximation for the average ZF SINR with respect to ray angles and phases, (25), follows.

C. Implications of the SINR Results

Equations (17) and (25) are powerful tools for interpreting the behaviour of ray-based massive MIMO channels.

MRC Processing: From (17), we observe the following key properties. As $\rho \to \infty$, the SINR reaches a ceiling from the residual interference always present with MRC. As $M \to \infty$, the SINR grows asymptotically linearly with M. A strong link gain, $\beta^{(l)}$, relative to $\beta^{(l')}$, $l' \neq l$, is clearly beneficial. Also, we observe that the spread of ray powers plays a role. In (17), large values of $\epsilon_c^{(l)}$ and $\epsilon_s^{(l)}$ improve the SINR. Using the result that $\nu_i = 1/n \, \forall i$ minimizes $\sum_{i=1}^{n} \nu_i^2$, it can be shown that minimum spread in the ray powers (i.e. a constant ray power) maximises both $\epsilon_c^{(l)}$ and $\epsilon_s^{(l)}$. Hence, spreading the link gain equally over the rays is beneficial, agreeing with our understanding that increased diversity increases performance.

The ray distribution affects the mean SINR through the K_c and K_s parameters. SINR grows linearly with K_s which is a function of ray variation within a cluster. Note that intra-cluster variation only affects the signal power so narrow angle spread within a cluster is beneficial as it creates many similar rays for the desired user which align to increase signal power. Inspection of (13) suggests that K_s increases with low angle spread and this is verified in Sec. V. The relationship of SINR to K_c is more complex. Differentiating (17) with respect to K_c we find that (17) is a decreasing function of K_c for typical operating parameters. The link between K_c and the actual angular PDF is not obvious as the K_c has a relatively complex formulation. Nevertheless, the trends can be inferred from the interpretation of K_c as the interference power between two distinct rays. For small numbers of antennas, traditional thinking applies. Angular PDFs with larger variance (wider angle spread) spread the rays, reducing the chance of two rays being similar and hence reducing interference. Therefore, increased angle spread is beneficial for small numbers of antennas. For large numbers of antennas, we use the initial formulation for K_c in (12), giving

$$K_c = E_\phi \left[\left| \sum_{m=0}^{M-1} \exp \left(j2\pi\delta m \left(\sin(\phi_{\hat{c},\hat{s}}^{(l)}) - \sin(\phi_{c,s}^{(l)}) \right) \right) \right|^2 \right]. \tag{26}$$

The maximum of the variable in (26) occurs at $\sin\phi_{c,s}^{(l)} = \sin\phi_{\hat{c},\hat{s}}^{(l)}$ so it is important to identify scenarios where very close agreement between the sines of the ray angles occurs. Since the sine function changes most rapidly around 0 (broadside), close agreement near broadside is less likely. However, the sine function changes least rapidly near $\pm\pi/2$ (end-fire) so here close agreement is more likely. This observation is more important for large M as $K_c \leq M^2$. Hence, for large numbers of antennas, increased angle spread puts more ray powers near to end-fire which inflates K_c. Thus, a cross-over occurs where larger angle spread increases SINR for smaller numbers of antennas and decreases SINR for larger numbers.

ZF Processing: The trends shown by (25) are the same as for MRC for M, K_c and the ray powers: asymptotic linear growth in M, a cross-over in the K_c behaviour and the desirability of large $\beta^{(l)}$ and small ray variation in the ray powers. The only different trend is the lack of a ceiling on the SINR as ρ increases due to the interference cancellation of perfect ZF. However, for MRC the K_c parameter scales the interference term, a dominant feature of MRC. In contrast, for ZF the K_c parameter appears in the denominator as a term which is $\mathcal{O}(L/M)$. Hence, the effect of K_c, and therefore the angular distributions, is less pronounced for ZF than for MRC.

IV. AVERAGING IN THE ANGULAR DOMAIN

The SINR expressions in (17) and (25) both require K_c which involves expectations of the form $\mathbb{E}_{\theta,\phi}[e^{jz\sin\phi}]$ where $z = 2\pi\delta m$, $m \in \mathbb{Z}$ and ϕ is the AoA of an arbitrary user's ray written as $\phi = \phi_c + \Delta$, where ϕ_c is the central cluster angle and Δ is the subray offset.

Lemma 1: We have $\mathbb{E}_\phi[e^{jz\sin\phi}] = \sum_{n=-\infty}^{\infty} \psi(n) J_n(z)$, where $\psi(n)$ is the characteristic function of ϕ, $\psi(n) = \mathbb{E}_\phi[e^{jn\phi}]$, and $J_n(.)$ is the nth order Bessel function of the first kind.

Proof: The proof is given in the Appendix. ∎

As the rays are modeled in clusters, we have

$$\psi(n) = \mathbb{E}_\phi[e^{jn\phi}] = \mathbb{E}_\phi[e^{jn(\phi_c + \Delta)}]$$
$$= \mathbb{E}_\phi[e^{jn\phi_c}]\mathbb{E}_{\theta,\phi}[e^{jn\Delta}] = \psi_c(n)\psi_s(n),$$

where $\psi_c(n)$ and $\psi_s(n)$ are the characteristic functions of the central cluster angles and subray offsets. From Lemma 1,

$$\mathbb{E}_\phi[e^{jz\sin\phi}] = \sum_{-\infty}^{\infty} \psi_c(n)\psi_s(n)J_n(z). \tag{27}$$

Note that (27) is completely general and applies to any clustered ray-based model where $\phi_{c,s} = \phi_c + \Delta_{c,s}$. Furthermore, in most cases the characteristic functions decay very rapidly so that (27) can be approximated by a small number of terms. For example, a common model is to have a wrapped normal distribution for ϕ_c, $\phi_c \sim \mathcal{N}(\mu_c, \sigma_c^2)$, and a

$$\mathbb{E}_{\theta,\phi}[\text{SINR}_l^{\text{ZF}}] \approx \frac{\rho M^2 \beta^{(l)2}}{K_c \left(L\frac{\beta^{(l)}}{M} - \frac{1}{M\beta^{(l)}} \sum_{c,s}^{C,S} \beta_{c,s}^{(l)2} \right) + M\beta^{(l)}} \qquad (25)$$

Laplacian for $\Delta_{c,s}$, $\Delta_{c,s} \sim \mathcal{L}(\frac{1}{\sigma_s})$, so that the PDF of $\Delta_{c,s}$ is $f_\Delta(x) = (2\sigma_S)^{-1} \exp(-|x|/\sigma_S)$. This choice gives the characteristic functions $\psi_c(n) = \exp(jn\mu_c - n^2\sigma_c^2/2)$ and $\psi_s(n) = (1 + n^2\sigma_s^2)^{-1}$. This specific solution gives

$$\mathbb{E}_\phi[e^{jz\sin\phi}] = \sum_{n=-\infty}^{\infty} \frac{e^{jn\mu_c - \frac{n^2\sigma_c^2}{2}}}{1 + n^2\sigma_s^2} J_n(z). \qquad (28)$$

Note that the coefficients of $J_n(z)$ behave like $n^{-2}\exp(-n^2\sigma_c^2/2)$ and therefore decay very quickly. Hence, a reasonable approximation may be obtained through $2N+1$ terms of the summation, giving

$$\mathbb{E}_\phi[e^{j2\pi\delta m\sin\phi}] \approx \sum_{n=-N}^{N} \frac{e^{jn\mu_c - \frac{n^2\sigma_c^2}{2}}}{1 + n^2\sigma_s^2} J_n(2\pi\delta m). \qquad (29)$$

Similarly, K_s in (14) requires the following result.

Lemma 2: We have

$$\mathbb{E}_\phi[\exp(jz(\sin\phi_{c,\hat{s}} - \sin\phi_{c,s}))]$$
$$= \sum_{n=-\infty}^{\infty} \sum_{m=-\infty}^{\infty} \psi_s(n)\psi_s^*(m)\psi_c(n-m)J_n(z)J_m(z). \qquad (30)$$

Proof: The proof follows similar arguments to Lemma 1 and is omitted for reasons of space. ∎

Substituting Lemmas 1 and 2 in (12) and (13) gives K_c and K_s which completes the derivation of (17) and (25).

V. NUMERICAL RESULTS

Unless otherwise stated, the numerical results were generated using parameter values in Table I. The users were randomly located in a cell of radius r, outside an exclusion radius r_0. The parameter ρ was chosen such that the tenth percentile of mean SNR, defined as $\text{SNR}_l = \frac{\rho\beta_l}{\sigma_n^2}$, was 0 dB. The cell wide performance statistics were computed for 10^4

TABLE I
PARAMETERS FOR NUMERICAL RESULTS

Parameter	Values
cell radius, r	100 m
exclusion radius, r_0	10 m
average SNR outage value	0 dB
average SNR outage probability	10%
pathloss exponent, Γ	3.2
shadow fading standard deviation, σ_{sf}	8.2 dB
link gain reference distance, d_0	1 m
number of users, L	10
number of clusters, C, (Scen. 1, Scen. 2)	3, 20
number of subrays, S, (Scen. 1, Scen. 2)	16, 20
cluster angle mean, μ_c	0°
cluster angle variance, σ_c^2, (Scen. 1, Scen. 2)	$(14.4°)^2$, $(76.5°)^2$
subray angle variance, σ_s^2, (Scen. 1, Scen. 2)	$(1.28°)^2$, $(15°)^2$

user locations ('drops') and the associated link gains, β_l in (2). Once the link gains are generated from (2), the cluster powers,

$\beta_c^{(l)}$, are set to decay exponentially from $\beta_1^{(l)}$ to $\beta_C^{(l)}$ in order to create unequal cluster powers. The inter-cluster ratio $\beta_C^{(l)}/\beta_1^{(l)}$ is set at 0.1 unless otherwise stated. Finally, all subpaths have the same power, so that $\beta_{c,s}^{(l)} = \beta_c^{(l)}/(CS)$. For each drop, the average over the ray angles and ray coefficient phases was evaluated using the appropriate analytical expression in Sec. III. These results were validated via simulation, where numerical averaging was performed over 10^3 angles drawn from the distribution described in Sec. IV. Hence, all performance metrics in Sec. V, such as SNR, signal power and interference power, are to be understood as the averaged values, where the averaging is over the ray angles and phases for a single drop of $\beta_{c,s}^{(l)}$ values. We consider the following two scenarios. Scenario 1, representing a relatively sparse channel with a narrow angular spread, is based on the recent measurement data in [5]. Scenario 2, which represents a rich scattering environment with a wide angular spread, is based on [7].

Fig. 1 shows the CDF of the ZF SNR (19), with the analytical results obtained via (25). In order to validate the approximations used in deriving (25), in addition to Scenarios 1 and 2, we consider extremely narrow angle spreads ($\sigma_c = 5°$, $\sigma_s = 2°$, $C = 3$, $S = 16$). We include results for $\mu_c = 0°$ and $\mu_c = 60°$. We consider $M = 150$. The results indicate that
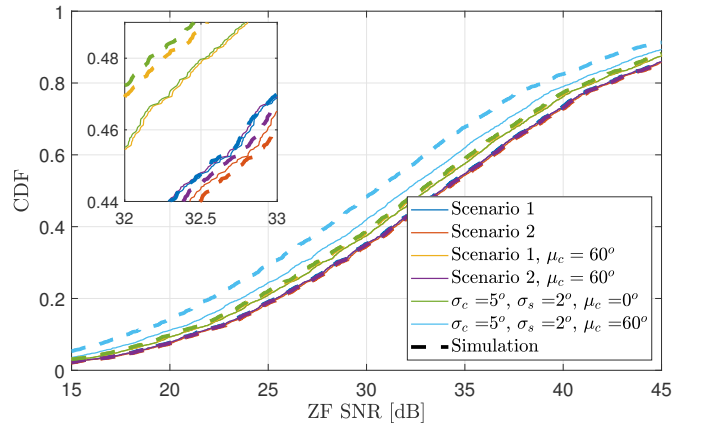

Fig. 1. ZF SNR CDF; Scen. 1, 2, and very narrow angle spreads; $M = 150$.

ZF SNR performance is very robust to changes in the channel parameters, with Scenarios 1 and 2 yielding nearly identical results. Closer examination of the CDFs in the figure inset shows that, as expected, the richer, more diverse environment of Scenario 2 slightly outperforms Scenario 1. This gap increases when the dominant direction moves away from array broadside, or when the scattering becomes extremely narrowly focused. The results also shows very high accuracy of (25) for all realistic parameter values. Only in the case of the extremely focused radiation, and near the array endfire, the Neumann series expansion leads to a noticeable approximation error.

Turning to MRC performance, in Fig. 2 we examine the distribution of the average signal power, with the analytical results in (14). The results are shown for $\mu_c = 0°$ with $M = 25$, 100 and 150 BS antennas. As with ZF SNR, MRC signal
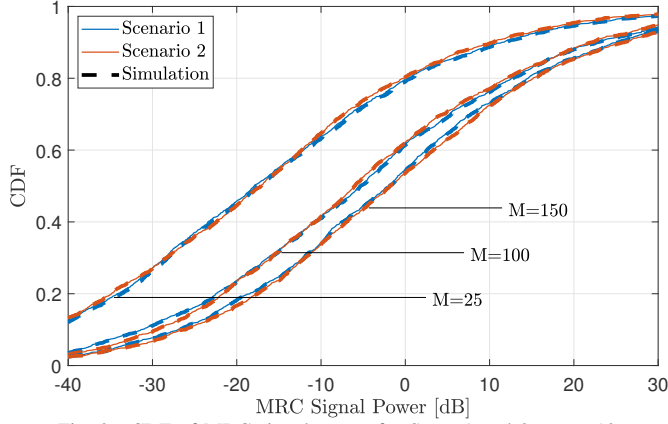

Fig. 2. CDF of MRC signal power for Scen. 1 and 2; $\mu_c = 0°$.

power is insensitive to the channel parameters, with Scenarios 1 and 2 resulting in nearly identical performance. While not shown to preserve figure clarity, the MRC signal strength also shows negligible sensitivity to changes in μ_c.

To demonstrate the robustness of the signal power to propagation characteristics, Fig. 3, shows the impact of the mean cluster angle μ_c on K_c and K_s in (17), and the effect of the cluster power distribution on ϵ_c and ϵ_s. The left subfigure
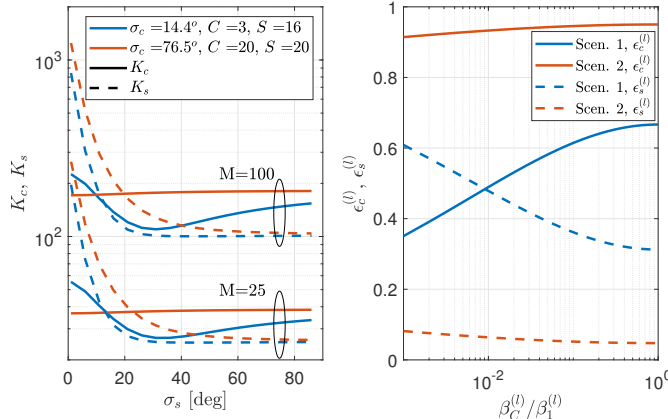

Fig. 3. MRC signal stability.

demonstrates that K_c and K_s have minor impact on the MRC signal power in (14). Constant K_s decays rapidly with increasing subray spread, as does K_c for Scenario 1. These constants scale ϵ_c and ϵ_s in (17), which relate to the spread of the cluster powers. The right subfigure plots ϵ_c and ϵ_s as a function of the inter-cluster power ratio, $\beta_C^{(l)}/\beta_1^{(l)}$. The change in ϵ_c and ϵ_s is small relative to the very large variation in $\beta_C^{(l)}/\beta_1^{(l)}$. Furthermore, the trend of the two variables is opposite, which further minimizes the variability of the signal power. As a result of these trends, and the dominance of M^2 in (14), the MRC signal power is robust to ray-based model parameters.

Next, we investigate the interference properties of MRC, which as per (15), is a function of K_c and the user link gains. We thus again focus on K_c. To add to the insights gained from Fig. 3, in Fig. 4 we plot K_c as a function of BS array size M. In order to more clearly illustrate the trends, we scale K_c by M. We observe that for small array sizes, the narrow angle spread results in larger interference than for wide angle spreads. However, the interference grows faster with M for wide angle spreads. As such, for large array size, the interference in the propagation environment of Scenario 2 dominates. Note that in order to demonstrate that the crossover effect can occur for realistic array size, in Fig. 4 we have shown Scenario 1 with a larger angle spread of $\sigma_s = 10°$. The
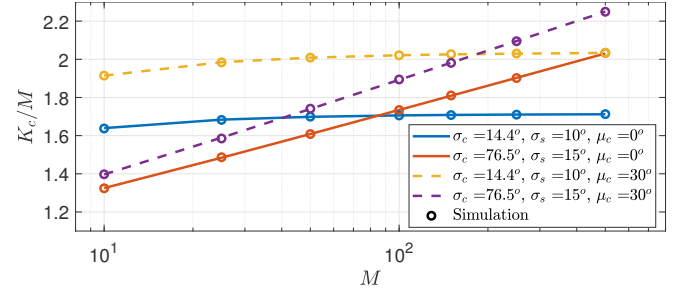

Fig. 4. Normalized MRC interference power.

trends observed in Fig. 4 confirm the predictions discussed in Sec III. Indeed, the cross-over occurs earlier for larger μ_c.

As discussed in Sec. III, a common approximation for the mean SINR for classical statistical models relies on the variance of the interference being small relative to its mean [16]. In order to establish the validity of such an approximation for ray-based models, we examine the variance of the interference in Fig. 5. In order to identify the impact on the interference variance of channel sparsity (C, S) and angular spread independently, in addition to the parameters of Scenarios 1 and 2, we also show two additional cases of sparse channels with wide angular spread and vice versa . Plotted for reference is the case of i.i.d. Rayleigh fading, as well as the variance normalised by $1/M^2$. The results clearly
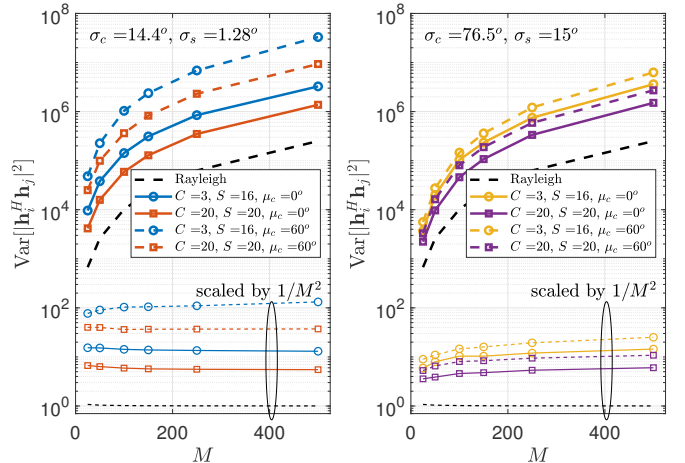

Fig. 5. MRC interference power variance.

demonstrate that the interference variance is much higher than that of a classical Rayleigh channel. We note that the variance is higher for channels with greater sparsity, and increases further as the propagation direction moves away from array broadside. These trends have a very important implication - the approximation for the expected SINR routinely used in the literature, should not be used for analyzing the performance of ray-based channels, unless higher order terms are considered.

Fig. 6 plots the ZF and MRC SINR as a function of M. In order to directly validate the trend predicted by (17) and (25), rather than computing cell-wide averaging, we consider a single random drop for each. As predicted by the analysis,
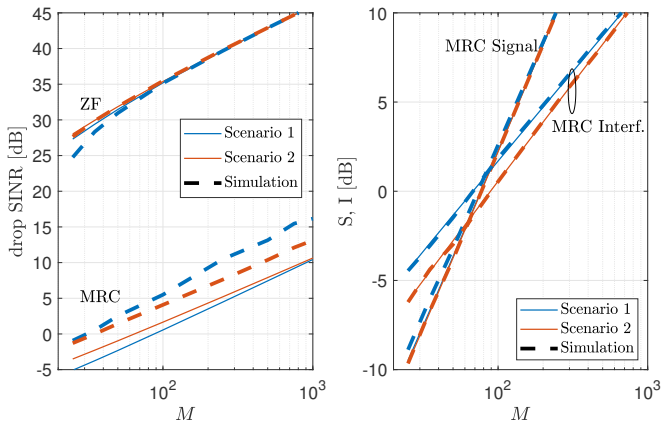

Fig. 6. ZF and MRC SINR. Results shown for an example drop.

both the ZF and MRC SINR grow linearly with M. We note that (25) is an accurate approximation to the simulated SNR for a wide range of M. As predicted by the analysis of MRC interference variance, the MRC SINR approximation is weak, in particular for the sparse Scenario 1. The right subfigure examines the corresponding signal and interference components. The approximations in (14) and (15) are shown to be extremely tight, confirming that the gap in the SINR approximation (17) is due to the first-order Laplace expansion.

VI. Conclusions

We have derived accurate expressions for the average ZF SNR and MRC signal, interference and noise powers. We have demonstrated that while ZF is robust to angular parameters, MRC interference is highly sensitive. Our closed form expressions show that the performance scales linearly with the number of antennas, and degrades with narrow angle spreads and as the propagation moves toward the antenna end-fire. Finally, we showed that the commonly used approximation for MRC SINR is inaccurate for ray-based analysis.

APPENDIX
PROOF OF LEMMA 1

Let $f(\phi)$ be the unwrapped PDF of ϕ and $f_w(\phi)$ be the wrapped PDF on $[-\pi, \pi]$. The required expectation is

$$\mathbb{E}_\phi[e^{jz\sin\phi}] = \int_{-\infty}^{\infty} e^{jz\sin\phi} f(\phi)d\phi = \int_{-\pi}^{\pi} e^{jz\sin\phi} f_w(\phi)d\phi.$$
(31)

Now, for any wrapped PDF [18], we have

$$f_w(\phi) = \frac{1}{2\pi} \sum_{n=-\infty}^{\infty} \psi(n)e^{-jn\phi},$$
(32)

where

$$\psi(n) = \mathbb{E}_\phi[e^{jn\phi}] = \int_{-\infty}^{\infty} e^{jn\phi} f(\phi)d\phi.$$
(33)

Hence,

$$\mathbb{E}_\phi[e^{jz\sin\phi}] = \int_{-\pi}^{\pi} e^{jz\sin\phi} \frac{1}{2\pi} \sum_{n=-\infty}^{\infty} \psi(n)e^{-jn\phi}d\phi$$

$$= \frac{1}{2\pi} \sum_{n=-\infty}^{\infty} \psi(n) \int_{-\pi}^{\pi} e^{j(z\sin\phi - n\phi)}d\phi.$$
(34)

The integral in (34) can be computed as

$$\int_{-\pi}^{\pi} e^{j(z\sin\phi - n\phi)}d\phi = 2\int_{0}^{\pi} \cos(z\sin x - nx)dx = 2\pi J_n(z),$$
(35)

using [19, pp. 452-453]. Hence the answer follows.

REFERENCES

[1] H. Tataria *et al.*, "Impact of line-of-sight and unequal spatial correlation on uplink MU-MIMO systems," *IEEE Wireless Commun. Lett.*, vol. 6, no. 5, pp. 634–637, Oct. 2017.

[2] ——, "On the general analysis of coordinated regularized zero-forcing precoding: An application to two-tier small-cell networks," *IEEE Trans. Commun.*, vol. 65, no. 7, pp. 3133–3150, Apr. 2017.

[3] ——, "Revisiting MMSE combining for massive MIMO over heterogeneous propagation channels," in *Proc. IEEE ICC*, Jun. 2018.

[4] O. Ozdogan *et al.*, "Uplink spectral efficiency of massive MIMO with spatially correlated Rician fading," in *Proc. IEEE SPAWC*, Jun. 2018, pp. 1–5.

[5] S. Sangodoyin *et al.*, "Cluster characterization of 3-D MIMO propagation channel in an urban macrocellular environment," *IEEE Trans. Wireless Commun.*, vol. 17, no. 8, pp. 5076–5091, Aug. 2018.

[6] M. R. Akdeniz *et al.*, "Millimeter wave channel modeling and cellular capacity evaluation," *IEEE J. Sel. Areas Commun.*, vol. 32, no. 6, pp. 1164–1179, Jun. 2014.

[7] 3GPP, "Study on channel model for frequencies from 0.5 to 100 GHz," 3rd Generation Partnership Project (3GPP), Tech. Rep. TR 38.901 (V14.0.0), Mar 2017. [Online]. Available: http://www.3gpp.org/

[8] C. T. Neil *et al.*, "Impact of microwave and mmWave channel models on 5G systems performance," *IEEE Trans. Antennas Propag.*, vol. 65, no. 12, pp. 6505–6520, Dec. 2017.

[9] X. Cheng and Y. He, "Channel modeling and analysis of ULA massive MIMO systems," in *Proc. IEEE ICACT*, Feb. 2018, pp. 411–416.

[10] X. Wu *et al.*, "On favorable propagation in massive MIMO systems and different antenna configurations," *IEEE Access*, vol. 5, pp. 5578–5593, 2017.

[11] Z. Gao *et al.*, "Asymptotic orthogonality analysis of time-domain sparse massive MIMO channels," *IEEE Commun. Lett.*, vol. 19, no. 10, pp. 1826–1829, Oct. 2015.

[12] J. Chen, "When does asymptotic orthogonality exist for very large arrays?" in *Proc. IEEE GLOBECOM*, Dec. 2013, pp. 4146–4150.

[13] C. Masouros and M. Matthaiou, "Space-constrained massive MIMO: Hitting the wall of favorable propagation," *IEEE Commun. Lett.*, vol. 19, no. 5, pp. 771–774, May 2015.

[14] H. Q. Ngo *et al.*, "Aspects of favorable propagation in massive MIMO," in *European Signal Process. Conf. (EUSIPCO)*, Sept 2014, pp. 76–80.

[15] N. Rupasinghe *et al.*, "Impact of angular spread in moderately large MIMO systems under pilot contamination," *IEEE Trans. Veh. Technol.*, 2018.

[16] Q. Zhang *et al.*, "Power scaling of uplink massive MIMO systems with arbitrary-rank channel means," *IEEE J. Sel. Topics in Signal Process.*, vol. 8, no. 5, pp. 966–981, Oct. 2014.

[17] D. Zhu *et al.*, "On the matrix inversion approximation based on Neumann series in massive MIMO systems," in *Proc. IEEE ICC*, Jun. 2015, pp. 1763–1769.

[18] K. V. Mardia, *Statistics of Directional Data*. Academic Press, 1972.

[19] N. M. Temme and D. Zwillinger, *Special Functions: An Introduction to the Classical Functions of Mathematical Physics*, 2nd ed. Wiley, 1996.